10

Whole-Body Fluorescence Imaging with Green Fluorescence Protein

Robert M. Hoffman

1. Introduction

1.1. Whole-Body Imaging of Green Fluorescent Protein-Expressing Tumors

Current methods for external imaging of internally growing tumors include X-rays, magnetic resonance imaging (MRI), and ultrasonography. Although these methods are well suited for the noninvasive imaging of large-scale structures in the human body, they have limitations in the investigation of internal, actively growing tumors. In particular, monitoring growth and metastatic dissemination by these methods is impractical, since they either use potentially harmful irradiation, or require harsh contrast agents, and therefore cannot be repeated on a frequent or real-time basis.

Previous attempts to endow tumors with specific, detectable spatial markers have mostly met with mediocre success. These included labeling with monoclonal antibodies and other high-affinity vector molecules targeted against tumor-associated markers *(1–6)*. However, results were limited as a result of achieving only a low tumor–background contrast, and because of the toxicity of the procedures.

Intravital videomicroscopy is another approach to optical imaging of tumor cells, which allows direct observation of cancer cells *(7)*. Even in this limited arena, intravital videomicroscopy does not lend itself to following tumor growth, progression, and internal metastasis in a live intact animal.

A major conceptual advance in optical imaging was to make the tumor the source of light. This renders the incident light scattering much less relevant. One early attempt inserted the luciferase gene into tumors, so that they emit

From: *Methods in Molecular Biology, vol. 183: Green Fluorescent Protein: Applications and Protocols*
Edited by: B. W. Hicks © Humana Press Inc., Totowa, NJ

light *(8)*. However, luciferase enzymes transferred to mammalian cells require the exogenous delivery of their luciferin substrate, an essentially impractical requirement in an intact animal. Also, it is not known whether luciferase genes can function stably over significant time periods in tumors and in the metastases derived from them.

A more practical approach to tumor luminance is to make the target tissue selectively fluorescent. In one attempt, tumor-bearing animals were infused with protease-activated, near-infrared fluorescent probes *(9)*. Tumors with appropriate proteases could activate the probes and be imaged externally. However, the system proved to have severe restrictions. The selectivity was limited, because many normal tissues have significant protease activity. In fact, the normal activity in liver is so high as to preclude imaging in this most important of metastatic sites. The short lifetime of the fluorescence probes would appear to rule out growth and efficacy studies *(9)*. The requirements of appropriate tumor-specific protease activity, and of effective tumor delivery of the probes, also limit this approach *(9)*.

A new approach of whole-body external imaging makes use of green fluorescent protein (GFP)-expressing tumors in intact animals. Stable GFP expression in cancer cells is an extremely effective marker *(10–18)*. The fluorescence illuminates tumor progression and allows visualization of tumor growth and metastases by whole-body imaging *(18)*. A major advantage of GFP-expressing tumor cells is that imaging requires no preparative procedures and are, therefore, uniquely suited for visualizing in live tissue *(10–18)*. Using stable GFP-expressing tumor cells *(10–18)*, external, noninvasive, whole-body, real-time, fluorescence optical imaging, is possible of internally growing tumors and metastases in transplanted animals *(18)*.

1.2. Whole-Body Imaging of GFP Gene Expression

Studies of gene expression in whole living animals involve spatial, as well as temporal and scalar, dimensions. The regional distribution of gene activity is of fundamental importance, as is the timing of response to physiological signals. Making such measurements in animals has been difficult. Every data point required sacrificing and dissecting the experimental animal and measuring the distribution of a reporter gene. Following a time-course in a single subject was, of course, impossible.

New techniques can visualize transgene expression noninvasively in intact animals, and promise a veritable revolution in genetic and physiological studies *(19–24)*. The methods are a significant extension of the century-old, noninvasive imaging of the internal tissues of intact animals. From Röntgen's X-rays to modern computed X-ray tomography and MRI, the static distribution of tissue mass has been visualized with ever-increasing resolution. Recent develop-

ments, such as MRI, have made possible visualizing dynamic processes. Now, noninvasive imaging has been extended to imaging the spatial distribution of transgene expression in living animals. Marker gene products have been visualized by MRI *(20,21)*, by emitted γ rays in micropositron emission tomography *(22)*, and single-photon emission computed tomography *(23)*, or by luciferin fluorescence *(24)*. Unfortunately, the procedures require complex and expensive apparatus, as well as the administration either of contrast agents or of substrates that are radioactive or fluorescent. Also, the signals are generally weak and so require long processing times, which limits detailed time-course measurements.

We have found that GFP can be used to visualize gene expression in small mammals *(25)*. Such imaging requires only that the gene under study or its promoter be coupled to GFP. The measurements are sufficiently rapid as to allow video recording for real-time measurements *(25)*.

2. Materials

2.1. Whole-Body Imaging Apparatus (see Note 1)

1. A Leica fluorescence stereo microscope, model LZ12, equipped with a 50 W mercury lamp, was used for high-magnification imaging. Selective excitation of GFP was produced through a D425/60 band-pass filter and 470 DCXR dichroic mirror. Emitted fluorescence was collected through a long-pass filter GG475 (Chroma Technology, Brattleboro, VT) on a Hamamatsu C5810 three-chip, thermoelectrically cooled, color charge-coupled device camera (Hamamatsu Photonics, Bridgewater, NJ).
2. Images were processed for contrast and brightness, and analyzed with the use of Image Pro Plus 3.1 software (Media Cybernetics, Silver Spring, MD).
3. Images of 1024 × 724 pixels were captured directly on an IBM PC, or continuously through video output on a high-resolution Sony VCR model SLV-R1000 (Sony, Tokyo, Japan).
4. Imaging at lower magnification, which visualized the entire animal, was carried out in a light box illuminated by blue light fiber optics (Lightools Research, Encinitas, CA) and imaged using the charge-coupled device camera described in **Subheading 1.**

2.2. Tumor Models and Gene Expression

1. 6-wk-old B57CL/6 or BALB/c *nu/nu* nude mice.
2. GFP-expressing tumor cells: Lewis lung carcinoma cells stably expressing GFP, murine melanoma B16F0-GFP.
3. Trypsin.
4. Ice-cold, serum-free modified Eagle's medium (MEM).
5. 1-mL latex-free syringe (Becton Dickinson, Franklin Lakes, NJ), 27- and 39-gauge needles.

6. GFP-expressing colon tumor fragments (1 mm^3).
7. 6-0, 7-0, and 8-0 surgical sutures.
8. Isoflurane anesthesia. Ketsel anesthesia.
9. 7X magnification microscope (Leica MZ6, Nussloch, Germany).
10. The adenovirus vector, AdCMV5GFPAE1/AE3 (vAd-GFP) (Quantum, Montreal, Canada), expressing enhanced green fluorescent protein and the ampicillin resistance gene.
11. Bone wax.
12. Sterile cotton

3. Methods

3.1. Tumor Models

3.1.1. Cell Injection

GFP-expressing cancer cells were made and isolated by growth in levels of Geneticin (G418) up to 800 µg/mL, as previously described *(15–18)*. The selected cancer cells have a strikingly bright GFP fluorescence that remains stable in the absence of selective agent after numerous passages. There is no difference in the doubling times of parental cells and GFP-expressing cells, as determined by comparison of proliferation in monolayer culture.

Metastasis in the brain, bone, liver, pancreas, lung and lymph nodes were externally imaged by GFP expression in intact mice *(18,31)*. External fluorescent images were acquired throughout the axial skeleton, including the skull, scapula, femur, tibia, and pelvis. A series of external fluorescence images of a tumor in the tibia were obtained from d-14 to d-25, after tail vein injection.

1. Harvest GFP-expressing tumor cells by trypsinization, using 0.25% trypsin for 3 min at 37°C.
2. Wash cells 3× with cold serum-free MEM.
3. Resuspend the cells in ~0.2 mL MEM.
4. Within 30 min of harvesting, inject 6-wk-old B57CL/6 or BALB/c *nu/nu* mice with 10^6 GFP-expressing tumor cells into the lateral tail vein, in a total volume of 0.2 mL, using a 1-mL 27G2 latex-free syringe (Becton Dickinson). External images from brain are shown in **Fig. 1**.
5. For liver expression (**Fig. 2**), cells can be injected directly into the portal vein.

3.1.2. Surgical Orthotopic Implantation

1. Perform all procedures of the operation under a 7× magnification microscope (Leica MZ6, Nussloch, Germany).
2. GFP-expressing tumor fragments (1 mm^3) are isolated by mincing tumor tissue that was growing subcutaneously in nude mice.
3. After proper exposure of the target organ, implant three tumor fragments per mouse.

14 days

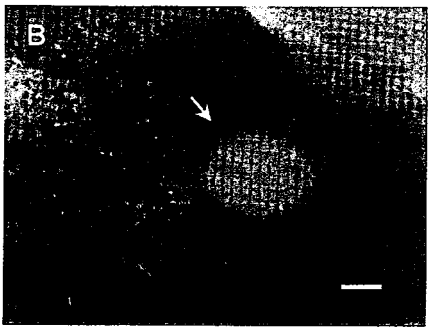

20 days

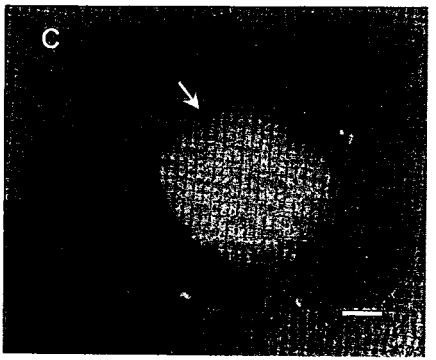

25 days

Fig. 1. External images of murine melanoma (B16F0-GFP) metastasis in brain *(18)*. Murine melanoma metastasis in the mouse brain were imaged by fluorescence microscopy using GFP expression, after injection of 10^6 B16F0-GFP cells in the tail vein. A clear image of a metastatic lesion in the brain can be visualized through the scalp and skull. **(A)** External image obtained of the tumor in the brain of nude mouse, d-14 after GFP tumor-cell injection. Bar = 1280 m. **(B)** Same as A, d-19 after injection. Bar = 1280 m. **(C)** Same as A and B, d-25 after injection. Bar = 1280 m. (For optimal, color representation please see accompanying CD-ROM.)

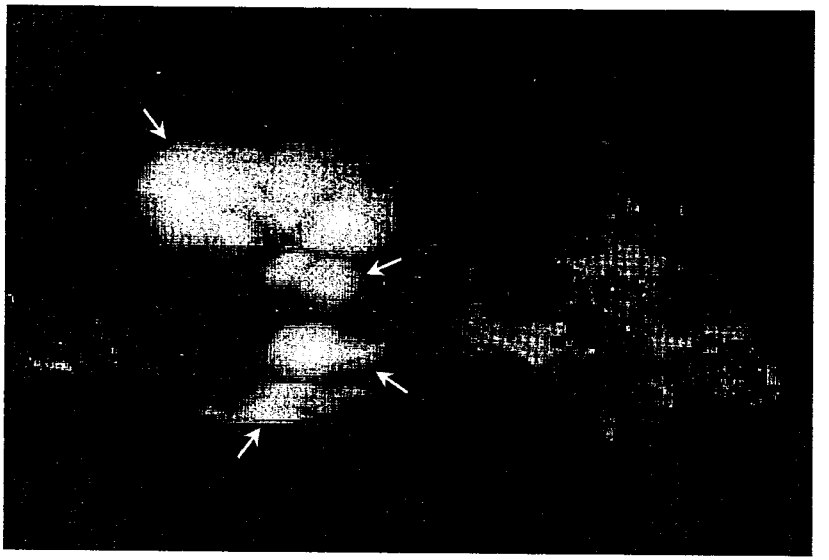

Fig. 2. External images of B16F0-GFP colonizing the liver *(18)*. Metastatic lesions of B16F0-GFP in the liver growing at a depth of 0.8 mm after portal vein injection. External image through the abdominal wall of the intact nude mouse. (For optimal, color representation please see accompanying CD-ROM.)

4. Using an 8-0 surgical suture, penetrate the tumor fragment, and suture the fragments onto the target organ.
5. Animals are kept in a barrier facility under high-efficiency particulate air filtration *(26)*.

3.1.3. Angiogenesis Model (see **Note 2**)

1. Inject Lewis lung carcinoma cells, stably expressing GFP subcutaneously, into a site of the footpad of 6-wk-old nude mice.
2. The relative transparency of the footpad reduces the scatter of green fluorescent light emitted from the tumor, and the relatively few resident blood vessels in the footpad makes it an excellent tumor transplantation site for tumor angiogenesis imaging.
3. The strong tumor cell GFP fluorescence contrasts well with the vessels, which are nonfluorescent, enabling their efficient imaging. The initiation of angiogenesis could be imaged externally when the tumor reaches approx 2 mm^2 *(31)*.

3.2. DNA Expression Models: Delivery of vAd-GFP to Various Organs for Whole-body Imaging (see Notes 3 and 4)

GFP expression in intact mice in the brain, liver, pancreas, prostate, and bone was externally imaged.

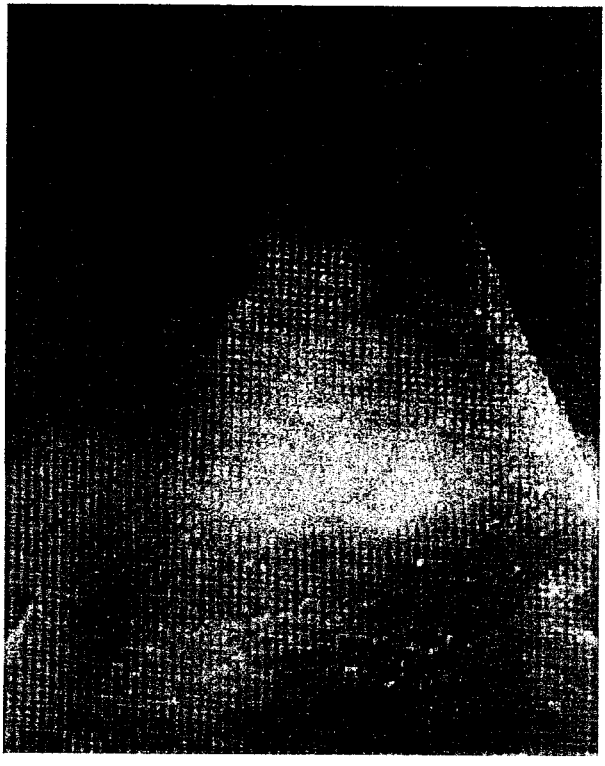

Fig. 3. External whole-body image of vAd-GFP gene expression in the brain *(25)*. An external image of vAd-GFP gene expression in the brain acquired from a nude mouse in the lightbox 24 h after gene delivery. Clear image of transgene expression in the brain can be visualized through the scalp and skull. (For optimal, color representation please see accompanying CD-ROM.)

3.2.1. Brain

1. The animals are kept under isofluorane anesthesia during surgery.
2. Following an upper midline scalp incision, expose the parietal bone of the skull.
3. Inject 20 μL recombinant adenovirus in phosphate-buffered saline (PBS), with 10% glycerol containing 8×10^{10} pfu/mL vAd-GFP/mouse, into the skull, using a 27G1/2 needle on a 1-mL latex-free syringe (Becton Dickinson).
4. Plug the puncture hole in the skull with bone wax.
5. Close the incision in the scalp with a 7-0 surgical suture in one layer.
6. Images can be collected beginning ~7 h after gene delivery (**Fig. 3**).

3.2.2. Liver

1. Keep the animals under Ketsel anesthesia during surgery.
2. The portal vein is exposed following an upper midline abdominal incision.

3. Inject 100 µL PBS with 10% glycerol containing 8×10^{10} pfu/mL vAd-GFP/mouse into the portal vein, using a 1-mL 39G1 latex-free syringe (Becton Dickinson).
4. For hemostasis, press the puncture hole in the portal vein with sterile cotton for ~10 s.
5. Close the incision in the abdominal wall with a 7-0 surgical suture in one layer.
6. All procedures of the operation described above were performed with a 7× magnification stereo microscope (Leica MZ12).

3.2.3. Pancreas

1. Keep the animals under Ketsel anesthesia during surgery.
2. All procedures of the operation described below are performed with a 7× magnification stereomicroscope.
3. Expose the pancreas following an upper midline abdominal incision.
4. Inject 100 µL PBS with 10% glycerol, containing 8×10^{10} pfu/mL vAd-GFP/mouse, into the pancreas, using a 39G1 needle on a 1-mL latex-free syringe (Becton Dickinson).
5. Press the puncture hole for ~10 s with sterile cotton for hemostasis.
6. Close the incision with a 7-0 surgical suture in one layer.

3.2.4. Prostate

1. Keep the animals under isoflurane anesthesia during surgery.
2. Expose the bladder and prostate, after making a lower midline abdominal incision.
3. Inject 30 µL PBS with 10% glycerol, containing 8×10^{10} pfu/mL vAd-GFP/mouse, into the prostate, using a 1-mL 39G1 latex-free syringe (Becton Dickinson).
4. Press the puncture hole in the prostate for ~10 s with sterile cotton for hemostasis.
5. Close the incision in the abdominal wall with a 6-0 surgical suture in one layer.
6. All procedures of the operation described above are performed with a 7× magnification stereomicroscope.

3.2.5. Bone Marrow

1. Anesthetize the animals by inhalation of isofluorane.
2. Open the skin on the hind leg with a 1-cm incision to expose the tibia.
3. A 27-gage needle with a 1-mL latex-free syringe (Becton Dickinson) is then inserted into the bone marrow cavity. Inject a total volume of 20 µL PBS with 10% glycerol (8×10^{10} pfu/mL) vAd-GFP/mouse into the bone marrow cavity.
4. Plug the puncture hole in the bone with bone wax and close the incision with a 6-0 surgical suture.

3.3. Measuring the Intensity of GFP Expression: Imaging Sensitivity and Resolution (see Note 5)

Estimating the intensity of GFP fluorescence is complicated by variations in the exciting illumination with time, and across the imaging area. These factors are corrected for by using the intrinsic red fluorescence of mouse skin as a base line to correct the increase over intrinsic green fluorescence caused by GFP *(25)*. This can be done because there is little red luminance in the GFP radiance. Consequently, the green fluorescence was calculated relative to red, based on red and green channel composition in the skin images *(25)*.

1. Produce a ratio (γ) of green to red channel emissions for each pixel in the images of skin without and with GFP.
2. Values of γ for mouse skin throughout the image in the absence of GFP should be fairly constant, varying between 0.7 and 1.0. The contribution of GFP fluorescence from within the animal increases the green component, compared to red, and is reflected in higher γ values.
3. Approximate the total amount of GFP fluorescence by multiplying the number of pixels in which the γ value was higher than 1× by the γ value of that pixel. Such a product roughly corresponds to the integral GFP fluorescence [I'_{GFP}] above the maximum value of γ for skin without GFP. The number of pixels in mouse skin images with γ value >1.0 without GFP was less than 0.02%.
4. GFP-expressing primary and metastatic lesions were considered to be externally measurable if the average fluorescence of the GFP-expressing tumor was at least 20% above the average fluorescence of the surrounding skin *(18)*. The level of background dorsal and abdominal skin fluorescence of nude mice was in a range of 6–9% of the exposed tumor fluorescence. The intensity of GFP fluorescence of a tumor (1 mm diameter) growing at a depth of ~0.8 mm was approx ~25% that of the exposed tumor. The minimum tumor size that could be imaged was a function of depth. The range of minimal size of GFP-expressing tumors that have been externally imaged thus far was from ~59 μm in diameter, at a depth of 0.5 mm, to ~1.86 mm in diameter, at a depth of 2.2 mm, in various tissues.
5. GFP transgene expression in various organs and tissues was considered to be externally measurable if the average fluorescence of the GFP-expressing organs was at least 20% above the average fluorescence of the surrounding skin *(25)*. The fluorescence intensity at maximal level of expression GFP in the liver exceeded more than 100× backdorsal and abdominal skin fluorescence. The intensity of GFP fluorescence of vAd-GFP expression in the mouse liver at a depth of 0.8 mm under the skin was approx ~25% of that of the exposed organ *(25)*.

3.4. Comparison of External Whole-Body Direct Images of GFP-Expressing Brain Metastasis

3.4.1. Comparison of Tumor Metastasis

A comparison was made between an external and direct image of a brain and metastasis of murine melanoma B16F0-GFP *(18)*.

1. Using a C57BL/6 mouse, inject 10^6 GFP-expressing B16F0-GFP tumor cells in 0.2 mL serum-free MEM into the tail vein.
2. Allow 25 d for tumor development.
3. Obtain an external fluorescent image (5.5 mm diameter and 0.8 mm depth) of B16F0-GFP cells through the scalp and skull of the mouse, on d 14, 19, and 25.
4. On d 25, after obtaining an external fluorescence image, dissect the animal, and remove the scalp and skull.
5. Record fluorescent images of the exposed brain for comparison.
6. The externally acquired images closely matched the images acquired from the open brain after the scalp and skull were removed. A series of external fluorescence images of the B16F0-GFP brain tumor in a single animal was obtained from d-14 to -25 after tail vein injection of B16F0-GFP in a nude mouse.
7. As determined by external imaging, the size of the metastatic lesion grew progressively with time (**Fig. 1**). The sizes of the tumors from external images at d 14, 19, and 25 were ~1.2, 2.25, and 3.5 mm, respectively.

3.4.2. Comparison of Viral Gene Expression in Liver

External images of vAd-GFP fluorescence from labeled mouse organs in living, intact animals were compared to the fluorescence of the organs viewed directly after sacrifice and dissection *(25)*. The fluorescence mapped the region of gene expression in the brain, liver, pancreas, prostate, and bone. The images made external to the animal appear similar to those of the exposed organs, reproducing much of the detailed structure of the direct image.

1. The simplest and most rapid method of obtaining whole-body fluorescent images of vAd-GFP gene expression is to place a freely moving mouse in a fluorescence light box (**Fig. 4**).
2. This system suggests the feasibility of high-throughput screening of agents that affect specific gene expression.

3.5. Real-Time Quantitative Whole-Body Imaging of vAd-GFP Gene Expression

Another important advantage of the GFP fluorescence assay for gene expression is its rapid data acquisition. Under the conditions used, images could be obtained at video rates, i.e., with exposure times in the order of one-thirtieth of a second *(25)*. The fluorescence from vAd-GFP gene expression in the brain of a single animal was visible within 6 h after local delivery of the vAd-GFP gene in a nude mouse, and by 24 h was very bright (**Fig. 3**). Liver fluorescence first became detectable at ~7 h after the injection of vAd-GFP into the tail vein *(25)*.

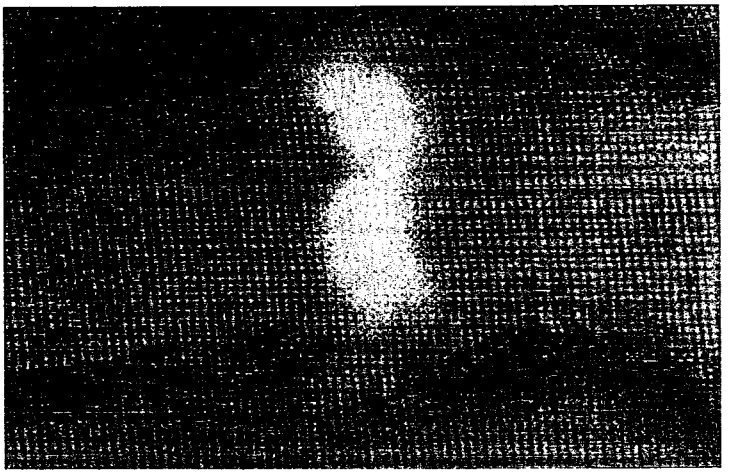

Fig. 4. External whole-body image of vAd-GFP gene expression in the liver *(25)*. An external image of vAd-GFP gene expression accquired from a nude mouse in the light box 72 h after gene delivery. Lateral, whole-body image of transgene expression in the liver can be clearly visualized through the abdominal wall. (For optimal, color representation please see accompanying CD-ROM.)

4. Notes

1. The GFP-based fluorescent optical tumor imaging system presents many powerful features *(18)*: Only the tumors and metastases contain the heritable GFP gene and are therefore selectively imaged with high intrinsic contrast to other tissues. GFP expression in the tumor cells is stable over long, indefinite time periods, which is the key feature allowing the quantitative imaging of tumor growth and metastasis formation, as well as their inhibition by agents of all types. The very bright GFP fluorescence enables internal tumors and metastases to be externally observed in critical organs such as colon, liver, bone, brain, pancreas, lymph nodes, and presumably breast, prostate, and so on. Blue-light illumination is the only requirement. No contrast agents, other chemical compounds, or additional treatments need to be administered to the animals.
2. Simultaneous, real-time, visual imaging of angiogenesis and tumor growth in intact animals is also enabled by establishment of human and rodent tumors that stably express high levels of GFP *(31)*. Vessels are highly visible by their natural contrast to the GFP expression in the tumor cells. The GFP whole-body imaging technology enables the quantitative imaging of the onset and development of tumor angiogenesis, which can be applied to high-throughput, in vivo screening of antiangiogenic agents.
3. vAd-GFP delivered to various organs was induced rapidly and was stable over long time periods, allowing real-time quantitative imaging of transgene expression *(25)*. These results indicate that gene induction and other kinetic studies can be visualized by whole-body imaging. The high intensity of GFP fluorescence

makes transgene expression externally observable from internal organs, including brain, liver, pancreas, prostate and bone and presumably in many other organs, such as breast, lymph nodes, and so on. No contrast agents, radioactive sources, or enzyme substrates need be administered to the animals; only blue-light illumination is necessary. The images can be acquired in real time, because of the strong GFP signal. The technology reported here can be applied to any gene or promoter fused or operatively linked to GFP in any organ.

4. We chose vAd-GFP as a vector, since it can transduce many normal tissues efficiently *(25)*. It was found that vAd-GFP gene is stably expressed in the brain and liver of nude mice at least for a number of months. Similar studies could be performed in transgenic animals in which GFP or other fluorescent proteins were fused or operatively linked to any gene or promoter.
5. Current sensitivity is limited, in part, by the nonoptimum spectrum of the GFP fluorescence (520 nm). At this relatively short wavelength, the emitted radiation is strongly scattered by surrounding tissue. However, powerful new techniques of using ultrafast lasers *(27)*, dual-photon imaging *(28)*, and ballistic photon imaging *(29,30)* may offer large gains in sensitivity, increased depth of detection, and spatial resolution.

References

1. Tearney, G. J., Brezinski, M. E., Bouma, B. E., et al. (1997) In vivo endoscopic optical biopsy with optical coherence tomography. *Science* **276,** 2037–2039.
2. Baum, P. R. and Brummendorf, T. H. (1998) Radioimmunolocalization of primary and metastatic breast cancer. *Q. J. Nucl. Med.* **42,** 33–42.
3. Teates, C. D. and Parekh, J. S. (1993) New radiopharmaceuticals and new applications in medicine. *Curr. Probl. Diagn. Radiol.* **22,** 229–226.
4. Dessureault, S. (1997) Pre-operative assessment of axillary lymph node status in patients with breast adenocarcinoma using intravenous ^{99}technetium mAb-170H. 82. *Breast Cancer Res. Treat.* **45,** 29–37.
5. Pasqualini, R., Koivunen, E., and Ruoslahti, R. (1997) Alpha v integrins as receptors for tumor targeting by circulating ligands. *Nat. Biotechnol.* **15,** 542–546.
6. Neri, D., Carnemolla, B., Nissim, A., et al. (1997) Targeting by affinity-matured recombinant antibody fragments on an angiogenesis associated fibronectin isoform. *Nat. Biotechnol.* **15,** 1271–1275.
7. Chambers, A. F., MacDonald, I. C., Schmidt, E. E., et al. (1995) Steps in tumor metastasis: new concepts from intravital videomicroscopy. *Cancer Metastasis Rev.* **14,** 279–301.
8. Sweeney, T. J., Mailander, V., Tucker, A. A., et al. (1999) Imaging brain structure and function, infection and gene expression in the body using light. *Proc. Natl. Acad. Sci. USA* **96,** 12,044–12,049.
9. Weissleder, R., Tung, C. H., Mahmood, U., Bogdanov, Jr., A. (1999) In vivo imaging of tumors with protease-activated near-infrared fluorescent probes. *Nat. Biotechnol.* **17,** 375–378.

10. Chishima, T., Miyagi, Y., Wang, X., et al. (1997) Cancer invasion and micrometastasis visualized in live tissue by green fluorescent protein expression. *Cancer Res.* **57,** 2042–2047.
11. Chishima, T., Miyagi, Y., Wang, X., Tan, Y., Shimada, H., Moossa, A. R., and Hoffman, R. M. . (1997) Visualization of the metastatic process by green fluorescent protein expression. *Anticancer Res.* **17,** 2377–2384.
12. Chishima, T., Miyagi, Y., Wang, X., et al. (1997) Metastatic patterns of lung cancer visualized live and in process by green fluorescence protein expression. *Clin. Exp. Metastasis* **15,** 547–552.
13. Chishima, T., Miyagi, Y., Li, L., et al. (1997) Use of histoculture and green fluorescent protein to visualize tumor cell host interaction. *In Vitro Cell Dev. Biol.-Anim.* **33,** 745–747.
14. Chishima, T., Yang, M., Miyagi, Y., et al. (1997) Governing step of metastasis visualized in vitro. *Proc. Natl. Acad. Sci. USA* **94,** 11,573–11,576.
15. Yang, M., Hasegawa, S., Jiang, P., et al. M. (1998) Widespread skeletal metastatic potential of human lung cancer revealed by green fluorescent protein expression. *Cancer Res.* **58,** 4217–4221.
16. Yang, M., Jiang, P., Sun, F.-X., et al. (1999) A fluorescent orthotopic bone metastasis model of human prostate cancer. *Cancer Res.* **59,** 781–786.
17. Yang, M., Jiang, P., An, Z., et al. (1999) Genetically fluorescent melanoma bone and organ metastasis models. *Clin. Cancer Res.* **5,** 3549–3559.
18. Yang, M., Baranov, E., Jiang, P., et al. (2000) Whole-body optical imaging of green fluorescent protein-expressing tumors and metastases. *Proc. Natl. Acad. Sci. USA* **97,** 1206–1211.
19. Herschman, H. R., MacLaren, D. C., Iyer, M., et al. (2000) Seeing is believing: noninvasive, quantitative and repetitive imaging of reporter gene expression in living animals, using positron emission tomography. *J. Neurosci. Res.* **59,** 699–705.
20. Louie, A. Y., Huber, M. M., Ahrens, E. T., et al. (2000) In vivo visualization of gene expression using magnetic resonance imaging. *Nat. Biotechnol.* **18,** 321–325.
21. Weissleder, R., Moore, A., Mahmood, U., et al. (2000) *In vivo* magnetic resonance imaging of transgene expression. *Nat. Med.* **6,** 351–354.
22. Gambhir, S. S., Barrio, J. R., Phelps, M. E., et al. (1999) Imaging adenoviral-directed reporter gene expression in living animals with positron emission tomography. *Proc. Natl. Acad. Sci. USA* **96,** 2333–2338.
23. Tjuvajev, J. G., Finn, R., Watanabe, K., et al. (1996) Noninvasive imaging of herpes virus thymidine kinase gene transfer and expressions potential method for monitoring clinical gene therapy. *Cancer Res.* **56,** 4087–4095.
24. Contag, P. R., Olomu, I. N., Stevenson, D. K., and Contag, C. H. (1998) Bioluminescent indicators in living mammals. *Nat. Med.* **4,** 245–247.
25. Yang, M., Baranov, E., Moossa, A. R., Penman, S., and Hoffman, R. M. (2000) Visualizing gene expression by whole-body fluorescence imaging. *Proc. Natl. Acad. Sci. USA* **97,** 12,278–12,282.

26. Fu, X., Besterman, J. M., Monosov, A., and Hoffman, R. M. (1991) Models of human metastatic colon cancer in nude mice orthotopically constructed by using histologically-intact patient specimens. *Proc. Natl. Acad. Sci. USA* **88,** 9345–9349.
27. Alfano, R. R., Demos, S. G., and Gayen, S. K. (1997) Advances in optical imaging of biomedical media. *Ann. NY Acad. Sci.* **820,** 248–270.
28. Masters, B. R., So, P. T., and Gratton, E. (1998) Multiphoton excitation microscopy of in vivo human skin. Functional and morphological optical biopsy based on three-dimensional imaging, lifetime measurements and fluorescence spectroscopy. *Ann. NY Acad. Sci.* **838,** 58–67.
29. Wu, J., Perelman, L., Dasari, R., and Feld, M. (1997) Fluorescence tomographic imaging in turbid media using early-arriving photons and Laplace transforms. *Proc. Natl. Acad. Sci. USA* **94,** 8783–8788.
30. Alfano, R. R., Demos, S. G., Galland, P., et al. (1998) Time-resolved and nonlinear optical imaging for medical applications. *Ann. NY Acad. Sci.* **838,** 14–28.
31. Yang, M., Baranov, E., Li, X.-M., et al. (2001) Whole-body and intra-vital optical imaging of angiogenesis in orthotopically implanted tumors. *Proc. Natl. Acad. Sci. USA* **98,** 2616–2621.
32. Bouvet, M., Yang, M., Nardin, S., et al. (2000) Chronologically-specific metastatic targeting models. *Clin. Experim. Metastat.* **18,** 213–218.